HHS Public Access

Author manuscript

Oral Oncol. Author manuscript; available in PMC 2018 August 01.

Published in final edited form as:

Oral Oncol. 2017 August ; 71: 156–162. doi:10.1016/j.oraloncology.2017.06.009.

Early detection of squamous cell carcinoma in carcinogen induced oral cancer rodent model by ratiometric activatable cell penetrating peptides

Dina V. Hingorani, PhD[1], **Aaron J. Lemieux, MD**[1], **Joseph R. Acevedo, BS**[1], **Heather L. Glasgow, PhD**[5], **Suraj Kedarisetty, MD**[1], **Michael A. Whitney, PhD**[2], **Alfredo A. Molinolo, MD**[3], **Roger Y. Tsien, PhD**[2,3,4], and **Quyen T. Nguyen, MD/PhD**[1,2,3]

[1]Division of Otolaryngology, Head and Neck Surgery, University of California, San Diego, La Jolla, CA, USA

[2]Department of Pharmacology, University of California, San Diego, La Jolla, CA, USA

[3]Moores Cancer Center, University of California San Diego, La Jolla, CA, USA

[4]Howard Hughes Medical Institute, University of California San Diego, La Jolla, CA, USA

[5]Department of Microbiology and Immunology, Albert Einstein College of Medicine, New York, NY, USA

Abstract

Objectives—Ratiometric cell-penetrating-peptides (RACPP) are hairpin-shaped molecules that undergo cleavage by tumor-associated proteases resulting in measurable Cy5:Cy7 fluorescence ratiometric change to label cancer *in-vivo*. We evaluated an MMP cleavable RACPP for use in the early detection of malignant lesions in a carcinogen-induced rodent tumor model.

Methods—Wild-type immune-competent mice were given 4-nitroquinoline-oxide (4NQO) for 16 weeks. Oral cavities from live mice that had been intravenously administered MMP cleavable PLGC(Me)AG-RACPP were serially imaged from week 11 through week 21 using white-light reflectance and Cy5:Cy7 ratiometric fluorescence.

Results—In an initial study we found that at week 21 nearly all mice (13/14) had oral cavity lesions, of which 90% were high-grade dysplasia or invasive carcinoma. These high-grade lesions were identifiable with white light reflectance and RACPP Cy5:Cy7 ratiometric fluorescence with similar detectability, Area Under Curve (AUC) for RACPP detection was 0.97 (95% Confidence interval (CI) = 0.92–1.02, $p<0.001$), sensitivity = 89%, specificity =100%. In a follow up study, oral cavity lesions generated by 4NQO were imaged and histologically analyzed at weeks 16,18

Corresponding author: Quyen T Nguyen, University of California San Diego, 9500 Gilman Drive, La Jolla CA 92093, Phone: 858-822-3965, Fax: 858-534-5270, q1nguyen@ucsd.edu.

Conflict of Interest: R.Y. Tsien, and Q.T. Nguyen are scientific advisors to Avelas Biosciences, which has licensed the ACPP technology from University of California Regents. No potential conflicts of interest were disclosed by the other authors.

and 21. In this study we showed that RACPP-fluorescence detection positively identified 15 squamous cell carcinomas (in 6 separate mice) that were poorly visible or undetectable by white light reflectance.

Conclusions—RACPP ratiometric fluorescence can be used to accurately detect carcinogen-induced carcinoma in immunocompetent mice that are poorly visible or undetectable by white light reflectance.

Introduction

Head and neck squamous cell carcinoma (HNSCC), which comprises cancer of the oral cavity, pharynx and larynx, is the 6th leading malignancy worldwide. With a reported annual burden of 633,000 incident cases, 355,000 deaths, and a 5 year overall survival rate ~ 60%, patient prognosis remains poor as diagnosis often occurs late into disease progression when advanced stage cancer is unresponsive to therapy [1–3]. Established risk factors for HNSCC include tobacco use and alcohol consumption [4]. Human Papilloma Virus (HPV) status has also been identified as a risk factor for HNSCC [5, 6]. Initial detection can present as ulcerations or exophytic growths with [7] conclusive diagnosis made by histological examination of biopsied lesions. Poor clinical diagnosis is partly due to the high degree of variability in visual presentation of lesions and the lack of simple reliable non-invasive methods to accurately identify potentially cancerous lesions.

A carcinogen induced mouse model of oral cavity cancer, (the most common type of HNSCC), has been reported using the addition of 4-nitroquinoline oxide (4NQO) to drinking water [10]. This chemical carcinogen promotes formation of DNA adducts similar to those induced by tobacco and other carcinogens. It has been shown that the activation of PIK3-AKT-mTOR pathway, which is a known precursor to MMP2 and 9 expression, occurs in this model. Mutations and change in expression of p53, which are also known precursors for elevated MMPs, were found in a rat model of 4NQO mediated SCCA [11]. At a cellular level, 4NQO induces various stages of carcinogenesis including dysplasia, neoplasia, in situ carcinoma, and squamous cell carcinoma (SCC) [12, 13]. For these reasons it is thought that such an animal model would better mimic the molecular pathogenesis of human disease compared to more widely used xenograft and transgenic animal models [14].

Matrix metalloproteinase-2 (MMP-2) and matrix metalloproteinase-9 (MMP-9) expression have been shown to correlate with cancer grade [15] and decreased patient survival [16, 17]. In carcinomas of the tongue, increased MMP2 and 9 expression correlates with an increased incidence of lymph node metastases [18]. Furthermore, the orthology of MMP 2 and 9 in human and mouse have been well established [19], suggesting that a molecular probe designed to detect these MMPs in animal models could be translated for clinical applications. Ratiometric ACPPs (RACPPs) undergo a change in the ratio of Cy5:Cy7 fluorescent emission upon cleavage by proteases. The cationic fragment of the RACPP is retained at the activation site, typically within the tumor. We have previously reported the use of MMP activatable cell penetrating peptides (ACPPs) probes for image guided surgery of tumors in various animal models of breast cancer [20], pancreatic cancer[21], melanoma and head and neck xenografts[22, 23]. We have also demonstrated significant correlation of

ratiometric fluorescence (Cy5:Cy7) from the MMP cleavable RACPP with tumor burden in a pancreatic tumor mouse model [21]. Concentration of other MMPs including, MMP 1 and 3 in human saliva and oral cancer are strong diagnostic markers oforal SCCA [8]. There is also some evidence to suggest that MMP7 gene expression is associated with early stages of oral cancer [9].

Here we report the use of serial MMP sensitive RACPP imaging to detect oral cavity SCCA induced by 4NQO in drinking water of mice. Additionally, we report the ability of MMP sensitive RACPP to highlight small SCCA lesions that are poorly visible or non-detectable using white light reflectance. The ability to detect SCCA before it becomes apparent on white light inspection suggests that this technology might be leveraged for early detection of SCCA of the head and neck.

Methods

All animal studies were approved by the UCSD Institutional Animal Care and Use Committee protocol #S04011.

Reagents

4NQO

Stock solution: A concentrated stock solution was made by dissolving 4NQO (Sigma Aldrich) in propylene glycol or DMSO (Sigma Aldrich) at a concentration of 4 mg/mL as previously described [10]. The stock solution was stored at 4°C and diluted into the drinking water at a final concentration of 50 μg/ml.

Vehicle: Initial experiments (Cohort 1) were performed with 4NQO dissolved in propylene glycol. During the course of the experiment, we noted that the use of propylene glycol as a vehicle for 4NQO delivery resulted in non-specific fluorescent signal in the dentition following injection of RACPP. To minimize this nonspecific signal, we tested stock solutions of 4NQO made in other solvents including ethanol (2mg/ml), PEG 300 (4mg/ml), DMSO (4mg/ml). The intensity of non-specific fluorescence signal of the dentition was greatest in mice given propylene glycol and least in mice given DMSO (Supplemental Fig. 1). Subsequent experimental animals (part of cohort 2) were administered with 4NQO using DMSO as vehicle.

RACPP—The peptide sequence H_2N-e_9-c(SS*t*Bu)-o-PLGC(Me)AG-r_9-c-amide was synthesized using standard FMOC chemistry. Peptide was purified by HPLC and reacted with Cy5-maleimide in presence of N-methylmorpholine (NMM) in dry DMSO. Following this, triethylphosphine (TEP) was added in excess for deprotection of the d-cysteine (i.e removal of –StBu to generate the thiol). This compound was precipitated in 80:20 hexane:EtOAc and purified by HPLC using a C18 column. Thereafter, the peptide was reacted with peg_{12}-maleimide (Quanta Biodesign) in presence of NMM followed by purification with HPLC. Peptide was then reacted with Cy7-NHS ester in dry DMSO with NMM for 24 hours to obtain MMP cleavable RACPP: (Cy7)-e_9-c(peg_{12})-o-PLGC(Me)AG-

r_9-c(Cy5) [24]. The selectivity of PLGC(Me)AG-RACPP for MMP2 and MMP9 and other related enzymes is highlighted in Supplemental Fig. 3.

Experimental model

In experimental cohort 1, 15 female C57Bl/6 mice, 4–6-weeks of age, weighing 18–20g, and 5 age, gender and species matched control mice were used. The 15 experimental mice were given 4NQO in their drinking water for 16 weeks while control mice were given vehicle only (Fig 1). At the end of 16 weeks, all mice were converted to drinking water without 4NQO and vehicle until the study endpoint at 21 weeks. One mouse died at week 7 for reasons unrelated to oral cavity tumor development and was excluded from analysis. Mice were evaluated for tumor growth every 2 weeks from week 11 to week 21. In each case the mice were anesthetized with isoflurane (2% in O_2) and the oral cavity was imaged using both white light reflectance and Cy5:Cy7 ratiometric fluorescence. Oral cavity examinations were performed ninety minutes after intravenous injection of 10 nmoles of MMP sensitive RACPP (Fig 2). Every lesion, location and size, was documented for each animal at each time-point for visibility by white light reflectance and Cy5:Cy7 ratiometric fluorescence. Transient lesions (i.e. present at one time point but not at subsequent time point) were believed to be due to minor trauma and were excluded from statistical analysis.

In cohort 2, 16 experimental mice were given 4NQO in their drinking water as described above for cohort 1. Having established a timeline for tumor growth, we endeavored to image animals in cohort 2 at early stages before the cancer becomes clearly visible by white light examination. Subsets of cohort 2, underwent oral cavity examination under anesthesia at various *single* time points followed by animal euthanasia and histologic analysis [weeks 16 (n = 6), week 18 (n = 4) and week 21 (n = 4)]. Intravenous administration of 20nmoles RACPP was followed by white light reflectance and Cy5:Cy7 ratiometric fluorescence imaging of the oral cavity as described in cohort 1 (Fig 1).

Histology

Following the final imaging session mice were euthanized for tissue harvest and histological analysis. The entire tongue from each mouse was dissected and placed on a platform to enable *ex vivo* measurements and correlation with *in vivo* imaging. Tongues were then flash-frozen for histological analysis. Sagittal 10 μm thick sections of the tongue were obtained using the Leica Cryostat (model CM1950) followed by staining with hematoxylin and eosin (H&E). All tissue samples were evaluated by a pathologist (AAM certified) blinded to the experimental conditions. Sections containing tumor and normal tissue were precisely identified based on their relative position on the whole tongues using both *in vivo* and *ex vivo* images (Fig 4C).

Image Analysis

All experimental animals underwent *in vivo* oral cavity examination using a modified Olympus OV100 small animal imaging system following intravenous injection of MMP-cleavable RACPP. The Olympus microscope is modified with continuous illumination with two light sources, a white visible light (400–650nm) and a NIR excitation source. The color or “reflectance” camera sees only the white-light image while the fluorescent camera sees

only the fluorophore's emission due to an appropriate long pass filter. Light emitting diodes are alternated at high speed, one for the white-light source and one for fluorescence source. Light collected by the system's main objective passes through a partially silvered mirror splitting the light between the two cameras. By restricting image integration to each camera's respective illumination interval, complete channel separation is achieved. The resulting image streams are processed, overlaid and displayed in real-time. Real-time video recordings under white light, Cy5 and Cy7 wavelengths were stored for analysis. Minimum and maximum signal settings are adjusted to obtain optimal contrast between area of interest and adjacent tissue and were kept consistent between samples to enable inter-sample comparisons. Images underwent post-processing using proprietary software developed in our lab to obtain optimal ratio of lesion to surrounding normal tongue contrast. Post-processing using our custom software made it easier to quantify Cy5:Cy7 ratios of the lesion. The in-house custom surgical microscope records and exports raw data files of each frame in all three channels i.e. Cy5 image, Cy7 image and white light color image. The 16 bit Cy5 image and Cy7 image of a specified frame (i.e. still-shot) are imported into the software simultaneously. The region of interest is selected with a mask function on the Cy5 image and the measure function reads out a value for the Cy5 signal intensity, Cy7 signal intensity of the same region and generates a ratio with a least count of 0.01. We have verified our values by analyzing the raw image files with Image J. For analysis with Image J, the Cy5 image is used to select the ROI with the free hand tool which is then saved using the ROI manager. The measured value of the Cy5 signal intensity is recorded. The Cy7 raw image of the same frame is now opened and the saved ROI is propagated into the image to measure the Cy7 signal intensity of the same area. A ratio of the two values gives the Cy5/Cy7 signal intensity of the region. Similar calculations are performed for the surrounding normal tongue using a concentric cylindrical shape with a width equal to the approximate diameter of the near spherical lesions. This was done to minimize the effect of non-specific signal from animal dentition (as a result of the vehicles propylene glycol or DMSO) on the adjacent oral tongue, a concentric ROI of the surrounding normal tongue around the lesion was measured to obtain the background ratiometric fluorescence A ratio of the Cy5:Cy7 ratio of the suspect lesion over the Cy5:Cy7 ratio of surrounding normal tongue gives the signal increase, where a value of 1 indicates no difference between suspect lesion and normal tongue.

Confocal imaging was obtained on tissue specimens sectioned at 10μm and cover slipped under phosphate buffered saline. A Nikon A1 confocal microscope (4X magnification and 0.20 numerical aperture objective) was used to obtain Cy5 and Cy7 confocal images with a 640nm laser. Image processing and Cy5:Cy7 tissue signal display was produced using Nikon NIS Elements software version 4.50. The number of lesions per animal was plotted as a function of time and stratified by lesion size beginning from initiation of 4NQO treatment (Figure 2, Figure 3A, C). Mice typically developed large visible lesions (2–4 mm) by week 17 with increasing frequency by week 21. New smaller lesions (<2mm) appeared consistently each week with the majority of mice (n = 13/14) having significant oral cavity lesions by week 21.

Statistics

Statistical analysis was performed using Microsoft Office Excel software and SPSS (version 19.0). The data are represented as means ± standard errors of the mean (SEM). Student t-test were computed to assess significant differences between groups. Paired and unpaired samples t-test were performed and one tail significance was set at $P<0.025$ for paired samples and two tail significance was set at $P<0.05$ for non-paired samples. Area under the curve (AUC) from baseline and receiver operator curves (ROC) were calculated using PRISM. Significance was set at $P<0.05$.

Results

RACPP ratiometric fluorescence detects lesions and their development over time as seen with white light reflectance

Ratiometric fluorescence imaging showed high uptake in lesions identified by white light reflectance (Fig 2B, Fig 3B). Of the lesions that showed high ratiometric fluorescence (n = 20), 70% (n = 14/20) were invasive SCCA, 20% (n = 4/20) were high grade dysplasia, and 10% (n = 2/20) were papillomas (Fig 3D). Using RACPP ratiometric analysis and a tumor/normal cutoff of 1.05, receiver operator curve (ROC) analysis for RACPP showed Area Under Curve (AUC) of 0.97 (95% Confidence interval (CI) = 0.92–1.02, p<0.001), sensitivity = 89%, specificity =100%. Tumors were equivalently detectable both in number and size using either white light inspection or ratiometric fluorescence. Although the majority of lesions detectable with RACPP ratiometric fluorescence were SCCA, a subset of lesions were dysplasia and papillomas. Unlike papillomas in human patients, papillomas that arise in this model usually evolve into SCCA [10].

Early detection of lesion by RACPP that are not visible using white light reflectance

To assess the ability of RACPP ratiometric fluorescence to detect SCCA that were not visible with white light, we imaged 16 mice at earlier time points prior to the development of large lesions that are easily visible by white light examination (Fig 1, **cohort 2**). Using ratiometric fluorescence imaging we identified 30 lesions (~0.2–2mm) in 75% (n=12/16) mice that could not be identified using white light reflectance alone. The remaining 4 mice did not have any surface lesions that were detected with either whitelight or ratiometric fluorescence. Of these, 15 lesions (50%, n=15/30) (Fig 4A–B) were confirmed as squamous cell carcinoma by histological analyses. These lesions had higher ratiometric fluorescence (4.6±1.4) compared to normal adjacent tongue (3.74±0.89) p<0.001; n=15, (Student's t test, paired, 1 tailed), Supplemental Video. AUC was 0.74 (95% CI = 0.55–0.93, p=0.026). At a cut off value of 4.45, sensitivity was 67% and specificity was 80%. Additional lesions with elevated ratiometric fluorescence were identified as pre-neoplasia (60%, n=9/15) and hyperplasia (40%, n=6/15) (Fig 5). These lesions also had higher ratiometric fluorescence compared to the adjacent normal tongue (Student's t test, paired, 1 tailed, p<0.001, n = 15). The average ratiometric fluorescence increase was 3 times higher for invasive SCCA lesions (21.02±12.36%, n=15) compared to pre-neoplasia/hyperplasia lesions (7.33±2.55%, n=15) p<0.001 Student's t test, non-paired, 2 tailed).

Discussion

HNSCC is a common cancer with poor survival, the incidence of which has steadily been increasing [25]. Diagnosis of HNSCC is often made at an advanced stage, partly due to the lack of reliable non-invasive methods to accurately identify malignant lesions [26–30]. Our lab has established the use of MMP sensitive RACPPs for image-guided surgery of tumors in various animal xenograft and transgenic models of breast cancer [20, 23], pancreatic cancer [21], melanoma and HNSCC [22]. In this study, we have successfully generated oral cavity SCC in an immunocompetent rodent model as previously described [10] and used established MMP responsive ratiometric fluorescence imaging, for comparative detection of cancerous lesions using white light inspection.

We found RACPP ratiometric fluorescence imaging can accurately identify SCCA lesions in this rodent model. Using a tumor/background ratio cut off of 1.05, we can differentiate between SCCA and surrounding normal tissue with 89% sensitivity and 100% specificity. We also found that RACPP ratiometric fluorescence imaging can identify very small lesions (<2mm) that were likely pre-cancerous and not easily detectable with white light reflectance. We were also able to identify both dysplastic and invasive SCCA lesions that were not visible with white light reflectance alone. Detectable but non-significant increases in MMP sensitive RACPP fluorescence was detected in low grade lesions. Inflammation and resulting immune cell infiltration could account for the MMP-mediated cleavage we see in these low grade lesions [31, 32]. MMP cleavable RACPPs are selective for MMP2 and MMP9 (Details of selectivity, Supplemental Fig 3) but they do not differentiate between MMPs produced by the tumor vs the stromal components. RACPP have also been shown to be internalized into tumor cells upon enzyme mediated cleavage [33, 34]. Interestingly, we found that the increased RACPP ratiometric fluorescence correlated with increasing histological evidence of tumor aggressiveness, i.e. invasive SCCA had higher ratiometric fluorescence compared to dysplasia which had increased ratiometric fluorescence compared to adjacent normal tissue.

In conclusion, we show that MMP-cleavable PLGC(Me)AG-RACPP ratiometric fluorescence imaging can be used to accurately identify invasive carcinoma lesions in a carcinogen induced rodent model of HNSCC. Although this is not a first “proof of concept study for MMP-cleavable RACPPs, it is the first study to show that RACPPs can be used to detect carcinogen induced lesions which more closely mimic HNSCC in humans. Future possible translation of PLGC(Me)AG-RACPP for HNSCC include intraoperative margin detection as well as in-office early detection of small lesions not conspicuous by examination with white light alone.

Supplementary Material

Refer to Web version on PubMed Central for supplementary material.

Acknowledgments

The authors would like to thank Susie Johnson for assistance with animal experiments, Paul Steinbach for computational and imaging support and Qing Xiong for peptide synthesis.

Funding

1. NIH (NIBIB) R01 EB014929-01 to QTN
2. NIH (NCI/NIBIB) 1R01CA158448-01A1 to RYT
3. NIH #1TL1 TR001443 to JRA

References

1. Ribeiro IP, Barroso L, Marques F, Melo JB, Carreira IM. Early detection and personalized treatment in oral cancer: the impact of omics approaches. Molecular Cytogenetics. 2016; 9:85. [PubMed: 27895714]
2. Schmidt H, Kulasinghe A, Kenny L, Punyadeera C. The development of a liquid biopsy for head and neck cancers. Oral Oncology. 2016; 61:8–11. [PubMed: 27688098]
3. Ferlay J, Shin HR, Bray F, Forman D, Mathers C, Parkin DM. Estimates of worldwide burden of cancer in 2008: GLOBOCAN 2008. Int J Cancer. 2010; 127:2893–917. [PubMed: 21351269]
4. Marur, S., Forastiere, AA. Mayo Clinic Proceedings. Elsevier; 2016. Head and neck squamous cell carcinoma: update on epidemiology, diagnosis, and treatment; p. 386-96.
5. Hennessey PT, Westra WH, Califano JA. Human papillomavirus and head and neck squamous cell carcinoma: recent evidence and clinical implications. Journal of dental research. 2009; 88:300–6. [PubMed: 19407148]
6. Gillison, ML. Seminars in oncology. Elsevier; 2004. Human papillomavirus-associated head and neck cancer is a distinct epidemiologic, clinical, and molecular entity; p. 744-54.
7. Jones KB, Jordan R. White lesions in the oral cavity: clinical presentation, diagnosis, and treatment. Seminars in cutaneous medicine and surgery. 2015; 34:161–70. [PubMed: 26650693]
8. Stott-Miller M, Houck JR, Lohavanichbutr P, Méndez E, Upton MP, Futran ND, et al. Tumor and salivary matrix metalloproteinase levels are strong diagnostic markers of oral squamous cell carcinoma. Cancer Epidemiology and Prevention Biomarkers. 2011; 20:2628–36.
9. Vairaktaris E, Serefoglou Z, Yapijakis C, Vylliotis A, Nkenke E, Derka S, et al. High gene expression of matrix metalloproteinase-7 is associated with early stages of oral cancer. Anticancer research. 2007; 27:2493–8. [PubMed: 17695544]
10. Czerninski R, Amornphimoltham P, Patel V, Molinolo AA, Gutkind JS. Targeting mammalian target of rapamycin by rapamycin prevents tumor progression in an oral-specific chemical carcinogenesis model. Cancer prevention research. 2009; 2:27–36. [PubMed: 19139015]
11. Osugi Y. p53 expression in various stages of 4-nitroquinoline 1-oxide induced carcinoma in the rat tongue. Journal of Osaka Dental University. 1996; 30:29–35. [PubMed: 9485768]
12. Kanojia D, Vaidya MM. 4-nitroquinoline-1-oxide induced experimental oral carcinogenesis. Oral Oncol. 2006; 42:655–67. [PubMed: 16448841]
13. Kim MM, Glazer CA, Mambo E, Chatterjee A, Zhao M, Sidransky D, et al. Head and neck cancer cell lines exhibit differential mitochondrial repair deficiency in response to 4NQO. Oral Oncol. 2006; 42:201–7. [PubMed: 16266817]
14. De Jong M, Maina T. Of mice and humans: are they the same?—Implications in cancer translational research. Journal of Nuclear Medicine. 2010; 51:501–4. [PubMed: 20237033]
15. Wittekindt C, Jovanovic N, Guntinas-Lichius O. Expression of matrix metalloproteinase-9 (MMP-9) and blood vessel density in laryngeal squamous cell carcinomas. Acta Otolaryngol. 2011; 131:101–6. [PubMed: 20873997]
16. Liu WW, Zeng ZY, Wu QL, Hou JH, Chen YY. Overexpression of MMP-2 in laryngeal squamous cell carcinoma: a potential indicator for poor prognosis. Otolaryngology--head and neck surgery: official journal of American Academy of Otolaryngology-Head and Neck Surgery. 2005; 132:395–400. [PubMed: 15746850]
17. Mallis A, Teymoortash A, Mastronikolis NS, Werner JA, Papadas TA. MMP-2 expression in 102 patients with glottic laryngeal cancer. Eur Arch Otorhinolaryngol. 2012; 269:639–42. [PubMed: 21667117]

18. Zhou CX, Gao Y, Johnson NW, Gao J. Immunoexpression of matrix metalloproteinase-2 and matrix metalloproteinase-9 in the metastasis of squamous cell carcinoma of the human tongue. Australian dental journal. 2010; 55:385–9. [PubMed: 21174909]
19. Jackson BC, Nebert DW, Vasiliou V. Update of human and mouse matrix metalloproteinase families. Human genomics. 2010; 4:194. [PubMed: 20368140]
20. Nguyen QT, Olson ES, Aguilera TA, Jiang T, Scadeng M, Ellies LG, et al. Surgery with molecular fluorescence imaging using activatable cell-penetrating peptides decreases residual cancer and improves survival. Proc Natl Acad Sci U S A. 2010; 107:4317–22. [PubMed: 20160097]
21. Metildi CA, Felsen CN, Savariar EN, Nguyen QT, Kaushal S, Hoffman RM, et al. Ratiometric Activatable Cell-Penetrating Peptides Label Pancreatic Cancer, Enabling Fluorescence-Guided Surgery, Which Reduces Metastases and Recurrence in Orthotopic Mouse Models. Ann Surg Oncol. 2014
22. Hauff SJ, Raju SC, Orosco RK, Gross AM, Diaz-Perez JA, Savariar E, et al. Matrix-metalloproteinases in head and neck carcinoma-cancer genome atlas analysis and fluorescence imaging in mice. Otolaryngol Head Neck Surg. 2014; 151:612–8. [PubMed: 25091190]
23. Hussain T, Savariar EN, Diaz-Perez JA, Messer K, Pu M, Tsien RY, et al. Surgical molecular navigation with a Ratiometric Activatable Cell Penetrating Peptide improves intraoperative identification and resection of small salivary gland cancers. Head Neck. 2014; 18:23946.
24. Savariar EN, Felsen CN, Nashi N, Jiang T, Ellies LG, Steinbach P, et al. Real-time in vivo molecular detection of primary tumors and metastases with ratiometric activatable cell-penetrating peptides. Cancer Res. 2013; 73:855–64. [PubMed: 23188503]
25. Chaturvedi AK, Engels EA, Pfeiffer RM, Hernandez BY, Xiao W, Kim E, et al. Human papillomavirus and rising oropharyngeal cancer incidence in the United States. Journal of clinical oncology: official journal of the American Society of Clinical Oncology. 2011; 29:4294–301. [PubMed: 21969503]
26. Kraft M, Fostiropoulos K, Gürtler N, Arnoux A, Davaris N, Arens C. Value of narrow band imaging in the early diagnosis of laryngeal cancer. Head & neck. 2016; 38:15–20. [PubMed: 24995546]
27. Stumpp P, Purz S, Sabri O, Kahn T. Molecular imaging of head and neck cancers: Perspectives of PET/MRI. Der Radiologe. 2016; 56:588. [PubMed: 27306200]
28. Di Martino E, Nowak B, Hassan HA, Hausmann R, Adam G, Buell U, et al. Diagnosis and staging of head and neck cancer: a comparison of modern imaging modalities (positron emission tomography, computed tomography, color-coded duplex sonography) with panendoscopic and histopathologic findings. Archives of Otolaryngology–Head & Neck Surgery. 2000; 126:1457–61. [PubMed: 11115282]
29. Cosway B, Drinnan M, Paleri V. Narrow band imaging for the diagnosis of head and neck squamous cell carcinoma: A systematic review. Head & neck. 2016
30. Muto M, Hironaka S, Nakane M, Boku N, Ohtsu A, Yoshida S. Association of multiple Lugol-voiding lesions with synchronous and metachronous esophageal squamous cell carcinoma in patients with head and neck cancer. Gastrointestinal endoscopy. 2002; 56:517–21. [PubMed: 12297767]
31. MacDougall JR, Matrisian LM. Contributions of tumor and stromal matrix metalloproteinases to tumor progression, invasion and metastasis. Cancer and Metastasis Reviews. 1995; 14:351–62. [PubMed: 8821095]
32. Heppner KJ, Matrisian LM, Jensen RA, Rodgers WH. Expression of most matrix metalloproteinase family members in breast cancer represents a tumor-induced host response. The American journal of pathology. 1996; 149:273. [PubMed: 8686751]
33. Olson ES, Aguilera TA, Jiang T, Ellies LG, Nguyen QT, Wong EH, et al. In vivo characterization of activatable cell penetrating peptides for targeting protease activity in cancer. Integrative Biology. 2009; 1:382–93. [PubMed: 20023745]
34. Jiang T, Olson ES, Nguyen QT, Roy M, Jennings PA, Tsien RY. Tumor imaging by means of proteolytic activation of cell-penetrating peptides. Proceedings of the National Academy of Sciences of the United States of America. 2004; 101:17867–72. [PubMed: 15601762]

Highlights

1. MMP sensitive RACPP-PLGC(Me)AG detects SCCA in an immune-competent carcinogen induced oral cancer mouse model.
2. RACPP-PLGC(Me)AG identifies cancer with excellent sensitivity and specificity.
3. RACPP-PLGC(Me)AG detects small cancerous lesions that are not visible by white light examination.
4. RACPP may be useful for intraoperative as well as non-invasive identification of cancer.

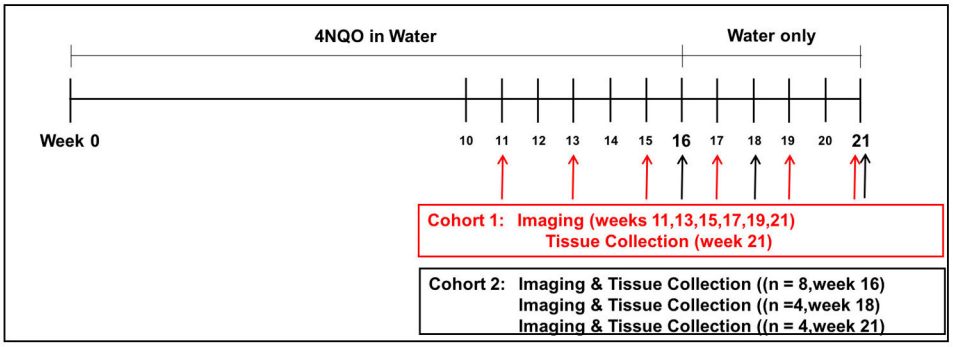

Figure 1. Experimental scheme. Cohort 1

A cohort of 14 mice were given 4NQO in their drinking water for 16 weeks at which time they were converted to regular drinking water until week 21. White light and ratiometric fluorescent (RF) imaging was done biweekly starting at 11 weeks, continuing until week 21 at which time tissue was collected for histological analysis. **Cohort 2:** A cohort of 16 mice were given 4NQO in their drinking water for 16 weeks followed by single time point imaging and tissue collection at week 16 (n=8), week 18 (n=4) and week 21 (n=4).

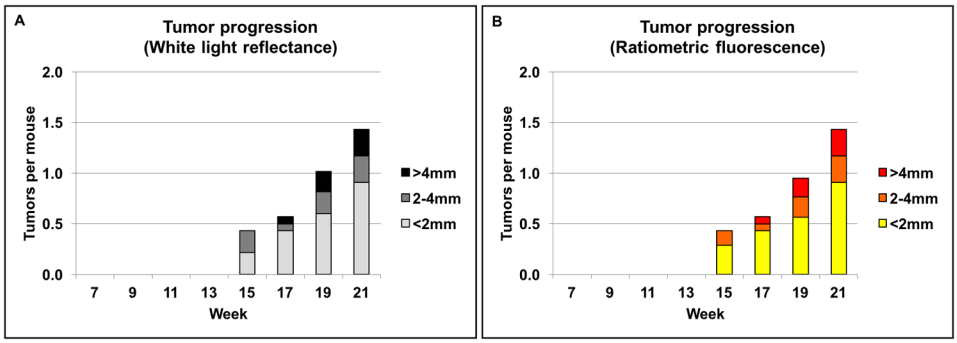

Figure 2. Tumor progression in cohort 1 (n=14)

Number of tumors and the tumor size distribution shown over time as detected by white light reflectance **(A)** and, Cy5:Cy7 ratiometric fluorescence **(B).** Tumor detected with white light and ratiometric fluorescence (RF) was similar in both number of tumors detected and size of individual tumors.

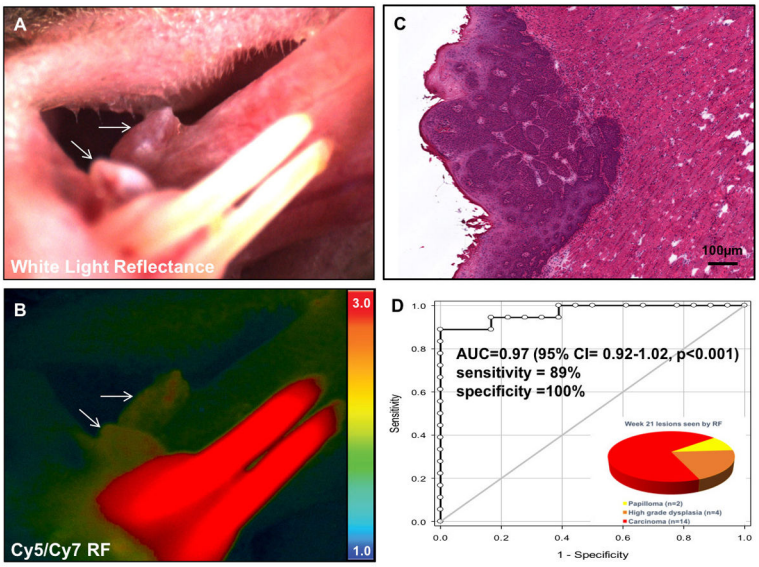

Figure 3. RACPP detects known exophytic cancer lesions

A. White light reflectance image showing a large exophytic lesion on the lateral tongue (white arrow) following chronic administration of 4NQO in the drinking water. **B.** Ratiometric fluorescent imaging following IV injection of RACPP-PLGC(Me)AG showing increased tumor uptake (white arrow) compared to adjacent tissue. High ratiometric fluorescence in the lower incisors is a nonspecific effect of the propylene glycol used to dissolve 4NQO. **C.** H&E image of the lesion in **A** and **B** showing invasive carcinoma. **D.** ROC curve for sensitivity and specificity of RACPPs (A=0.97). Inset: Distribution of lesions visualized by ratiometric fluorescence at week 21. Each lesion was categorized by their most severe pathology. Carcinoma was the most common, followed by high grade dysplasia and papilloma (a low grade dysplasia).

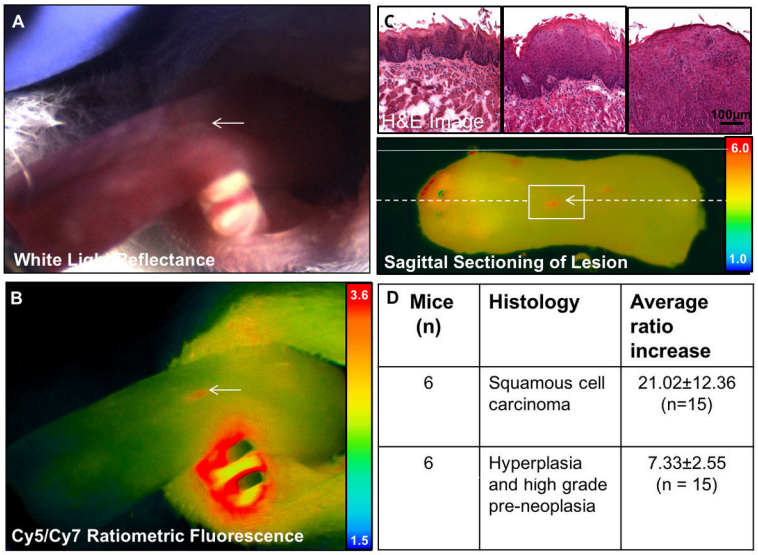

D

Mice (n)	Histology	Average ratio increase
6	Squamous cell carcinoma	21.02±12.36 (n=15)
6	Hyperplasia and high grade pre-neoplasia	7.33±2.55 (n = 15)

Figure 4. MMP cleavable RACPP detects SCCA not detectable by white light

A. Dorsal tongue with marked location (white arrow) showing no clear signs on cancer on white light examination **B.** Ratiometric fluorescence shows increase in Cy5:Cy7 ratio compared to adjacent tissue due to MMP mediated cleavage of RACPP. **C.** H&E image at the level of boxed region in C showing that the lesion seen in A and B is an invasive carcinoma (third column). There is adjacent low grade and high grade dysplasia in the surrounding tissue (first and second columns). Ex vivo ratiometric fluorescence image showing position on excised tongue and serial sectioning used to confirm pathology of small lesion detected by ratiometric fluorescence. Solid white line shows the position of the lateral tongue edge and stippled white line shows the sagittal section across the lesion. **D.** Summary table of lesions with corresponding histology that are seen by ratiometric fluorescence but not by white light inspection of the tongue.

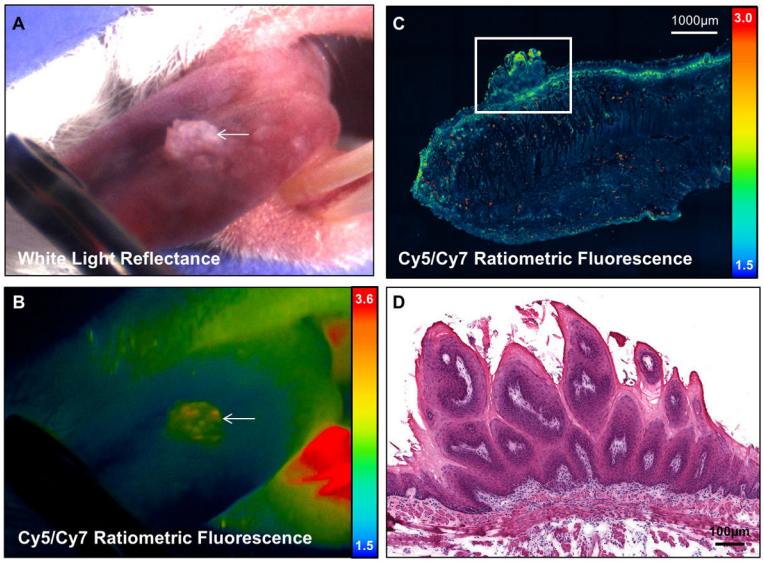

Figure 5. Papilloma detectable by white light reflectance with low RACPP signal

A. Color image under white light and **B.** pseudo-color ratiometric fluorescence image showing a large lesion on the dorsal tongue (arrow) in a wild type mouse. **C.** Confocal image of a sagittal section of tissue across the lesion. There is some evidence of chronic inflammation in the superficial stroma indicated by high fluorescence signal. **D.** H&E image at the level of boxed region in C showing that the lesion in A and B features benign hyperkeratosis and hyperplasia with finger-like stromal expansion characteristic of papilloma.